

## Layered and laterally constrained 2D inversion of resistivity data

Esben Auken\* and Anders Vest Christiansen\*

### ABSTRACT

In a sedimentary environment, quasi-layered models often can represent the actual geology more accurately than smooth minimum-structure models. We present a 2D inversion scheme with lateral constraints and sharp boundaries (LCI) for continuous resistivity data. All data and models are inverted as one system, producing layered solutions with laterally smooth transitions. The models are regularized through lateral constraints that tie interface depths or thicknesses and resistivities of adjacent layers. A priori information, used to resolve ambiguities and to add, for example, geological information, can be added at any point of the profile and migrates through the lateral constraints to parameters at adjacent sites. Similarly, information from areas with well-resolved parameters migrates through the constraints to help resolve areas with poorly constrained parameters. The estimated model is complemented by a

full sensitivity analysis of the model parameters supporting quantitative evaluation of the inversion result.

A simple synthetic model proves the need for a quasi-layered, 2D inversion when compared with a traditional 2D minimum-structure inversion. A 2D minimum-structure inversion produces models with spatially smooth resistivity transitions, making identification of layer boundaries difficult.

A continuous vertical electrical sounding field example from Sweden with a depression in the depth to bedrock supports the conclusions drawn from the synthetic example. A till layer on top of the bedrock, hidden in the traditional inversion result, is identified using the 2D LCI scheme. Furthermore, the depth to the bedrock surface is easily identified for most of the profile with the 2D LCI model, which is not the case with the model from the traditional minimum-structure inversion.

### INTRODUCTION

Standard electrical methods allow for a detailed mapping by gathering profile-oriented data continuously using either multiple electrode systems (Dahlin, 1996; Bernstone and Dahlin, 1999) or various pulled systems (Sørensen, 1996; Panissod et al., 1997). These systems provide a dense profile-oriented data coverage with large sensitivity overlaps between individual soundings. This naturally invites 2D interpretations. Since 1994, inversion algorithms have been presented by Oldenburg and Li (1994) and Loke and Barker (1996). These algorithms produce smooth minimum-structure models in which sharp formation boundaries are often hard to recognize. A robust inversion scheme (L1 norm) tends to give a more blocky appearance of the model section (Loke et al., 2001), but layer boundaries are still smeared.

In many instances the investigator may suspect a predominantly layered subsurface, as is most often the case in sedimentary environments or for most hydrogeological investigations (Christensen and Sørensen, 1998). The situation is often as

presented in Figure 1. An interpreter has an inversion result as presented in Figure 1a and needs to make a geological interpretation. The geology is layered in some sense, but the formation boundaries must be visualized based on the rather smooth and smeared inversion result. A possible interpretation might look like Figure 1b. Later we will return to this example and show that it is preferable to use an inversion scheme utilizing a layered model description.

Often a 1D solution with lateral constraints is sufficient in quasi-layered sedimentary environments (Auken et al., 2002). However, neotectonics, glacioteconics, or other geological phenomena may disturb the subhorizontal layering, disqualifying the 1D formulation to describe the geophysical model. So, a 2D formulation is needed to enable a more complex layered-earth solution.

Olayinka and Yaramanci (2000) present a 2D block inversion scheme using polygons of equal resistivity. They invert for positions of polygon vertices and for the polygon resistivities. As is the case for most 2D programs, no sensitivity analysis on model parameters accompanies the inversion output. Smith

Manuscript received by the Editor April 1, 2003; revised manuscript received December 10, 2003.

\*University of Aarhus, HydroGeophysics Group, Department of Earth Sciences, Finlandsgade 6-8, DK-8200 Aarhus N, Denmark. E-mails: esben.auken@geo.au.dk; anders.vest@geo.au.dk.

© 2004 Society of Exploration Geophysicists. All rights reserved.

et al. (1999) present a sharp boundary inversion for MT data using a 2D formulation. They use a layered earth discretized along a profile with lateral interpolation between neighboring nodes. The model is regularized using lateral constraints on layer conductivities and depths.

We have adapted the model description used by Smith et al. (1999) to be used in a 2D inversion program for resistivity data. The inversion is based on an algorithm developed for a 1D inversion scheme using lateral constraints on resistivities, depths, or thicknesses (LCI). The 1D LCI approach produces pseudo 2D models when lateral resistivity variations are smooth (Auken et al., 2002). A priori information can be added at any point of the profile; information migrates through the lateral constraints to the adjacent nodes. The inversion result is supported by a full sensitivity analysis of the model parameters that is essential to ascertain the quality of the inversion result. The inversion scheme is tested and compared to a standard 2D smooth inversion on both synthetic data and field data.

#### DATA ACQUISITION SYSTEMS

Field examples given in this paper are based on data acquired with the continuous vertical electrical sounding (CVES) system and the pulled array continuous electrical sounding (PACES) systems.

The CVES system consists of a number of steel electrodes manually forced into the ground at regular electrode spacing, typically from 2 to 12 m (Van Overmeeren and Ritsema, 1988; Dahlin, 1996). The electrodes function as both current and potential electrodes and can measure in any configuration desired by the user. The data collecting is semicontinuous using a roll-along technique.

The PACES system consists of a small tractor, equipped with processing electronics, pulling the electrodes mounted on a

tail (Sørensen, 1996). The electrodes are cylindrical steel tubes weighing about 15 kg. Two electrodes are maintained as current electrodes; the remaining electrodes serve as potential electrodes in eight different configurations. The data collection is continuous at approximately 1.5 m/s, with one full sounding saved each second and later processed to one sounding for every 5.0 m.

#### INVERSION METHODOLOGY

##### Data and model

Consider a data set consisting of  $\rho_a$ , apparent resistivity data collected along the profile assembled in a data vector:

$$\mathbf{d}'_{obs} = (\rho_{a1}, \rho_{a2}, \dots, \rho_{aN})^T, \quad (1)$$

where  $T$  indicates the vector transpose and  $N$  is the number of data points. Thus,  $\mathbf{d}'_{obs}$  is a column vector. To minimize nonlinearity and to impose positivity, we apply logarithmic data and logarithmic parameters as in Johansen (1977) and Ward and Hohmann (1987). Hence,

$$\mathbf{d}_{obs} = (\log(\rho_{a1}), \log(\rho_{a2}), \dots, \log(\rho_{aN}))^T. \quad (2)$$

The data vector has an observational error  $\mathbf{e}_{obs}$  which we suppose is unbiased, meaning that the expectation value is zero. Then the covariance matrix,  $\mathbf{C}_{obs}$ , has the elements

$$C_{obs,st} = \text{cov}(\mathbf{e}_{obs,s}, \mathbf{e}_{obs,t}) \quad (3)$$

for the  $s$ th and  $t$ th data error.

The derivation of the inversion formalism applies for the general case. However, in this paper we assume the observational errors to be uncorrelated so that  $\mathbf{C}_{obs}$  is a diagonal matrix. The model has  $n_x$  reference node points  $x_i$  in the horizontal direction corresponding to the data profile. At each surface node  $x_i$ , the subsurface model is represented by a logarithmic model with  $n_l$  layers:

$$\mathbf{m}_i = (\log(\rho_{i1}), \log(\rho_{i2}), \dots, \log(\rho_{in_l}), \log(t_{i1}), \log(t_{i2}), \dots, \log(t_{i(n_l-1)}))^T, \quad (4)$$

where  $\rho$  denotes interval resistivity and  $t$  denotes interval layer thickness. The full model

$$\mathbf{m} = \begin{pmatrix} m_1 \\ m_2 \\ \vdots \\ m_{n_x} \end{pmatrix} \quad (5)$$

to be determined has  $M = n_x * (2n_l - 1)$  parameters. The parameters from neighboring nodes are interpolated linearly to produce a 2D model as illustrated in Figure 2.

##### Forward modeling

The 2D forward modeling in the inversion routine is performed using the finite-difference code from the University of British Columbia (McGillivray, 1992), similar to the one described by Dey and Morrison (1979). We superimpose the finite-difference grid on the layered model as shown in

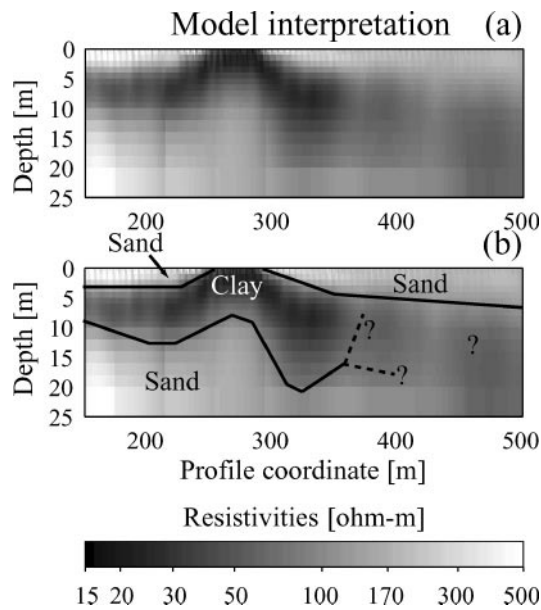


Figure 1. (a) An L2 norm inversion (Oldenburg and Li, 1994) of a continuous resistivity data set. (b) A possible geological interpretation drawn on top of the inversion result. The interpreter assumed the subsurface to be layered.

Figure 3a. Then we assign a resistivity value to each cell based on an area weighted average of the contributing elements in the underlying layered 2D model (Figure 3b).

Electrodes are placed on node points in the grid. For irregular electrode configurations, we implement a linear interpolation on the electrode positions to the two nearest nodes to avoid rounding odd positions. Systems with irregular electrode configurations inevitably mean dense finite-difference grids. This, in combination with profiles of the order of kilometers, makes it practically impossible to calculate all forward responses with one large grid. Instead, we divide the profile into pieces and calculate for each piece on its own, afterward combining them to create the full profile. The choice of the subgrid sizes can reduce the computation time drastically. The choice is based on the total size of the profile and the smallest and largest electrode spreads. Because of computational costs, the grid size should be limited to 10 000 cells, keeping in

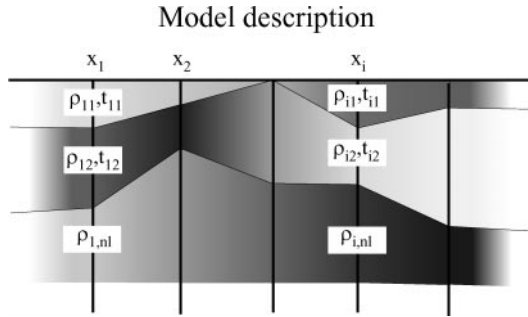


Figure 2. The model is described with thicknesses and resistivities at a number of nodes along a profile. The parameters between neighboring nodes are linearly interpolated to produce a 2D model.

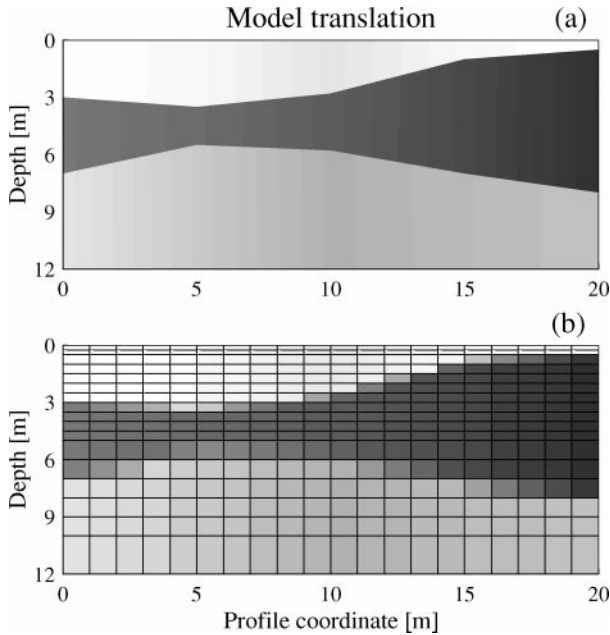


Figure 3. The layered model in (a) is translated to the model superimposed on the finite-difference grid in (b) using weighted averages.

mind that the overlap between neighboring pieces needs to be sufficiently large to ensure continuous forward data along the profile.

### Forward mapping

The dependence of apparent resistivities on subsurface parameters is in general described as nonlinear differentiable forward mapping. We follow the established practice of linearized approximation by the first term of the Taylor expansion:

$$\mathbf{d}_{obs} \cong \mathbf{g}(\mathbf{m}_{ref}) + \mathbf{G}(\mathbf{m}_{true} - \mathbf{m}_{ref}) + \mathbf{e}_{obs}, \quad (6)$$

where  $\mathbf{g}$  is the nonlinear mapping of the model to the data space. The true model  $\mathbf{m}_{true}$  has to be sufficiently close to some arbitrary reference model  $\mathbf{m}_{ref}$  for the linear approximation to be good. In short, we write

$$\delta \mathbf{d}_{obs} = \mathbf{G} \delta \mathbf{m}_{true} + \mathbf{e}_{obs}. \quad (7)$$

The Jacobian  $\mathbf{G}$  contains all of the partial derivatives of the mapping

$$G_{st} = \frac{\partial d_s}{\partial m_t} = \frac{\partial \log(\rho_{as})}{\partial \log(m_t)} = \frac{m_t}{\rho_{as}} \frac{\partial \rho_{as}}{\partial m_t}, \quad (8)$$

for the  $s$ th apparent resistivity in the data vector and the  $t$ th parameter in the model vector.

### A priori and lateral constraints on primary parameters

The inclusion of lateral constraints is based on an approach used for 1D LCI. Because the methodology builds on the 1D case, we distinguish between primary parameters (thicknesses and resistivities) and secondary parameters (in this case, depths). A priori information helps resolve the nonuniqueness of the model and is a way to include information not originating from the resistivity data itself. Following Jackson (1979), a priori information on primary parameters is included as an extra data set  $\mathbf{m}_{prior}$ :

$$\mathbf{I} \delta \mathbf{m}_{true} = \delta \mathbf{m}_{prior} + \mathbf{e}_{prior}, \quad (9)$$

where  $\delta \mathbf{m}_{prior} = \mathbf{m}_{prior} - \mathbf{m}_{ref}$ . Effectively,

$$\mathbf{I} \mathbf{m}_{true} = \mathbf{m}_{prior} + \mathbf{e}_{prior}, \quad (10)$$

where  $\mathbf{e}_{prior}$  is the error on the a priori model with zero as the expected value and  $\mathbf{I}$  is the identity matrix with the dimension of the model vector. The variance in the a priori model is described in the covariance matrix  $\mathbf{C}_{prior}$ .

Next, we add roughening constraints to the solution. Formally, the constraints are connected to the true model as

$$\mathbf{R}_p \delta \mathbf{m}_{true} = \delta \mathbf{r}_p + \mathbf{e}_{rp}, \quad (11)$$

where, subscript  $p$  denotes primary parameters,  $\mathbf{e}_{rp}$  is the error on the constraints with zero as expected values, and

$$\delta \mathbf{r}_p = -\mathbf{R}_p \mathbf{m}_{ref}, \quad (12)$$

making the effective roughening

$$\mathbf{R}_p \mathbf{m}_{true} + \mathbf{e}_{rp} = 0. \quad (13)$$

The roughening matrix  $\mathbf{R}_p$  contains 1 and  $-1$  for the constrained parameters and zero in all other places, such that

$$\mathbf{R}_p = \begin{bmatrix} 1 & 0 & \cdots & 0 & -1 & 0 & \cdots & 0 & 0 & 0 \\ 0 & 1 & 0 & \cdots & 0 & -1 & 0 & \cdots & 0 & 0 \\ \vdots & & & & \vdots & & & & \vdots & \\ 0 & 0 & 0 & \cdots & 0 & 1 & 0 & \cdots & 0 & -1 \end{bmatrix}. \quad (14)$$

The variance, or strength of the constraints, is described in the covariance matrix  $\mathbf{C}_{Rp}$ . In this study  $\mathbf{C}_{Rp}$  is taken to be a diagonal matrix. For most applications only constraints between neighboring models are used but can be between any two sub-models. Normally we use only lateral constraints, but vertical constraints (Farquharson and Oldenburg, 1998) can be applied as well. Applying both vertical and horizontal constraints results in a minimum structure model.

#### A priori depth values and lateral constraints

For many applications, lateral constraints on depths are advantageous to constraints on thicknesses. Constraints on thicknesses are favorable whenever there is a possibility of discontinuous layer boundaries but continuous thicknesses, such as across a fault. Constraints on depths are preferred in cases where we have a demand for continuity of layer boundaries, as in a Quaternary sequence with sand and clay layers on top of a relatively smooth pre-Quaternary surface.

The inverse solution is formulated in terms of the primary model parameters. This means that a priori information on depths is added with respect to the primary parameters in  $\mathbf{m}_{true}$ :

$$\mathbf{P}_h \delta \mathbf{m}_{true} = \delta \mathbf{m}_{h-prior} + \mathbf{e}_{h-prior}, \quad (15)$$

where

$$\delta \mathbf{m}_{h-prior} = \mathbf{h}_{prior} - \mathbf{P}_h \mathbf{m}_{ref}, \quad (16)$$

so that effectively

$$\mathbf{P}_h \mathbf{m}_{true} = \mathbf{h}_{prior} + \mathbf{e}_{h-prior}. \quad (17)$$

The matrix  $\mathbf{P}_h$  is derived in Appendix A. The vector  $\mathbf{h}_{prior}$  contains the values to which we constrain individual depths:

$$\mathbf{h}_{prior} = (\log(h_{1,1}), \dots, \log(h_{n_x, n_l-1}))^T \quad (18)$$

in which  $h_{ij}$  is the a priori depth number  $j$  in the model number  $i$ . The error on the a priori data is  $\mathbf{e}_{h-prior}$ , with zero as the expected value. The variance in the a priori data is described in the covariance matrix  $\mathbf{C}_{h-prior}$ , where  $\mathbf{C}_{h-prior}$  is taken to be a diagonal matrix.

For the lateral constraints on depths, we need to derive the equations with respect to the primary parameters in  $\mathbf{m}_{true}$ :

$$\mathbf{R}_h \delta \mathbf{m}_{true} = \delta \mathbf{r}_h + \mathbf{e}_{rh}, \quad (19)$$

where  $\mathbf{e}_{rh}$  is the error on the depth constraints with zero as the expected value and

$$\delta \mathbf{r}_h = -\mathbf{R}_h \mathbf{m}_{ref}, \quad (20)$$

making the effective roughening

$$\mathbf{R}_h \mathbf{m}_{true} + \mathbf{e}_{rh} = 0. \quad (21)$$

The derivation of the  $\mathbf{R}_h$  can be found in Appendix A.

#### Inversion

By joining equations (7), (9), (11), (15), and (19), we can write the inversion problem as

$$\begin{bmatrix} \mathbf{G} \\ \mathbf{I} \\ \mathbf{P}_h \\ \mathbf{R}_p \\ \mathbf{R}_h \end{bmatrix} \cdot \delta \mathbf{m}_{true} = \begin{bmatrix} \delta \mathbf{d}_{obs} \\ \delta \mathbf{m}_{prior} \\ \delta \mathbf{m}_{h-prior} \\ \delta \mathbf{r}_p \\ \delta \mathbf{r}_h \end{bmatrix} + \begin{bmatrix} \mathbf{e}_{obs} \\ \mathbf{e}_{prior} \\ \mathbf{e}_{h-prior} \\ \mathbf{e}_{rp} \\ \mathbf{e}_{rh} \end{bmatrix}. \quad (22)$$

We write this more compactly as

$$\mathbf{G}' \cdot \delta \mathbf{m}_{true} = \delta \mathbf{d} + \mathbf{e}'. \quad (23)$$

The covariance matrix  $\mathbf{C}'$  for the joint observation error  $\mathbf{e}'$  becomes

$$\mathbf{C}' = \begin{bmatrix} \mathbf{C}_{obs} & & & & \\ & \mathbf{C}_{prior} & & & \\ & & \mathbf{C}_{h-prior} & & \\ & & & \mathbf{C}_{Rp} & \\ & & & & \mathbf{C}_{Rh} \end{bmatrix}. \quad (24)$$

The model estimate (Menke, 1989)

$$\delta \mathbf{m}_{est} = [\mathbf{G}'^T \mathbf{C}'^{-1} \mathbf{G}']^{-1} \mathbf{G}'^T \mathbf{C}'^{-1} \delta \mathbf{d}' \quad (25)$$

minimizes

$$Q = \left( \frac{1}{N + M + A} \sum_{i=1}^{N+M+A} [(\delta \mathbf{d}'^T \mathbf{C}'^{-1} \delta \mathbf{d}')] \right)^{\frac{1}{2}}, \quad (26)$$

where  $N$  is the number of data points,  $A$  is the number of constraints, and  $M$  is the number of model parameters, including depths. When only diagonal error covariances are used, as in this paper, the misfit criterion simplifies to

$$Q = \left( \frac{1}{N + M + A} \sum_{i=1}^{N+M+A} \left[ \frac{\delta \mathbf{d}'_i^2}{\text{var}(\mathbf{e}'_i)} \right] \right)^{\frac{1}{2}}. \quad (27)$$

The target misfit for the 2D LCI is in principle zero, which in practice means as low as possible within the computational limits. This would be considered huge overfitting for an underdetermined smooth inversion problem. But for a parameterized and overdetermined problem as the 2D LCI, we have found that this is not the case. On account of the restricted number of parameters, the inversion scheme cannot make models arbitrarily complex. This is furthermore restricted by the lateral constraints. The full iterative inversion scheme is given in Appendix B.

### Analysis of model estimation uncertainty

The parameter sensitivity analysis of the final model is the linearized approximation to the covariance of the estimation error  $\mathbf{C}_{est}$  (Tarantola and Valette, 1982) given by

$$\mathbf{C}_{est} = (\mathbf{G}'^T \mathbf{C}'^{-1} \mathbf{G}')^{-1}. \quad (28)$$

Including all subterms, this becomes

$$\mathbf{C}_{est} = (\mathbf{G}'^T \mathbf{C}_{obs}^{-1} \mathbf{G}' + \mathbf{C}_{prior}^{-1} + \mathbf{P}_h^T \mathbf{C}_{h-prior}^{-1} \mathbf{P}_h + \mathbf{R}_p^T \mathbf{C}_{Rp}^{-1} \mathbf{R}_p + \mathbf{R}_h^T \mathbf{C}_{Rh}^{-1} \mathbf{R}_h)^{-1}. \quad (29)$$

Standard deviations on model parameters are calculated as the square root of the diagonal elements in  $\mathbf{C}_{est}$ . For mildly nonlinear problems this is a good approximation. Because the model parameters are represented as logarithms, the analysis gives a standard deviation factor (STDF) on the parameter  $q_s$ , defined by

$$\text{STDF}(q_s) = \exp(\sqrt{C_{est(s,s)}}). \quad (30)$$

Hence, under a lognormal assumption, it is 68% likely that a given model parameter  $q$  falls in the interval

$$\frac{q}{\text{STDF}_q} < q < q \cdot \text{STDF}_q. \quad (31)$$

Thus, the impossible case of perfect resolution has an STDF of one. An STDF of 1.1 is approximately equivalent to an error of 10%. Moderate to well-resolved parameters have an STDF less than 1.5, poorly resolved parameters an STDF less than 2, and mainly unresolved parameters an STDF greater than 2.

### SYNTHETIC EXAMPLE

To demonstrate the need for a 2D inversion code utilizing layered models, we compare results from a simple synthetic model. The data set is generated using the PACES electrode configuration, with one sounding per meter, each comprising eight data points. These data points then have had 3% noise added and processed to one sounding for each 5 m. The processing steps are identical to those taken for real data.

The model in Figure 4a is a three-layer earth representing a typical sedimentary environment with clay interbedded in sand. The model scenario is typical for groundwater surveys

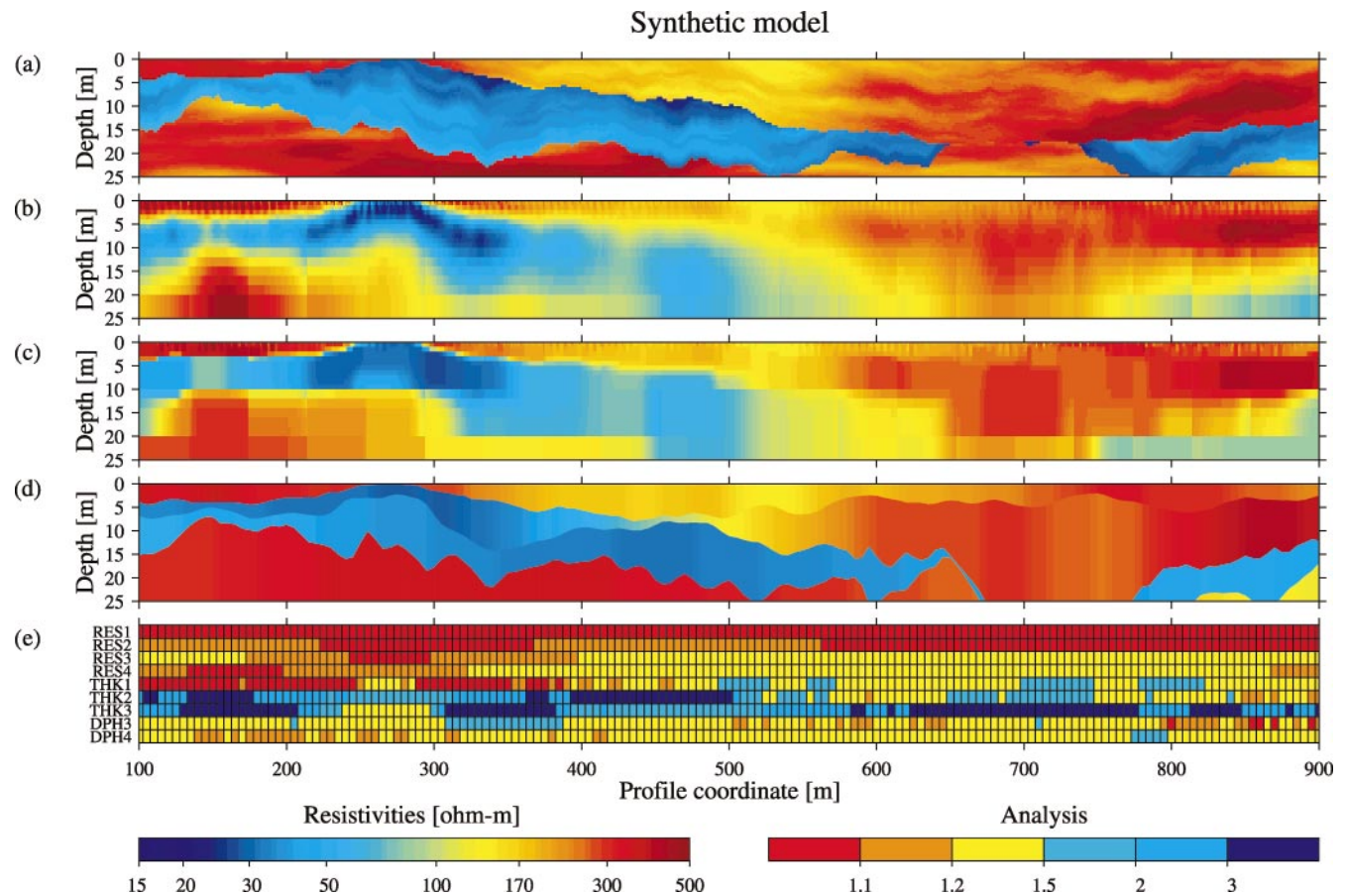


Figure 4. (a) The true model, with a clay layer of 30 ohm-m interbedded in a sandy layer of 300 ohm-m. (b) The minimum structure L2 norm inversion result. (c) The corresponding L1 norm inversion result. (d) The 2D LCI result. (e) An analysis of the model parameters (resistivities, RES1-RES4; thicknesses, THK1-THK3; and depths, DPH3-DPH4). The analysis uses a six-graded color code ranging from red (well determined) to blue (undetermined).

where we wish to map protective clay layers. The layer boundaries and internal resistivity variations are set using the result of stationary stochastic processes characterized by the von Karman covariance functions (Møller et al., 2001). Mean layer resistivities are 300 ohm-m, 30 ohm-m, and 300 ohm-m for the three layers, respectively. The internal standard deviation on resistivities is 0.5 times the logarithm to the resistivity. Mean interval thicknesses of the first and second layers are 5 and 10 m, respectively. The standard deviation on the thicknesses is equal to the mean value.

We use the code by Oldenburg and Li (1994) for comparison. It can perform strict L1 norm and L2 norm inversions.

The L2 norm inversion in Figure 4b finds the basic near-surface features but has difficulties in tracking the deeper parts of the low-resistivity layer. Also, it fails to recognize the resistivity transitions as sharp boundaries between the layers in the true model. This is most pronounced in the deeper parts of the model where the resolution capabilities are modest.

When applying an L1 norm misfit criterion as in Figure 4c instead of the usual L2 norm misfit criterion, the model appearance becomes more blocky, with sharp resistivity transitions both laterally and vertically (Loke et al., 2001; Farquharson and Oldenburg, 2003). However, these sharp transitions do not reproduce the actual boundary transitions in the true model.

The 2D LCI inversion in Figure 4d is carried out with equal size constraints on layer resistivities and on the layer boundaries, i.e., depths to layers. The constraint on resistivities is a factor of 1.1 (matrix  $C_p$ ), and on depths it is a factor of 1.3 (matrix  $C_{Rh}$ ). These values are fairly general and have been tested on a wide variety of models (initially established by trial and error). With these settings we find both the correct geometry and the layered nature of the model for the near surface and the deeper parts of the model. The model sections presented produce data that fit the observed data to an acceptable level according to the relevant inversion scheme.

The four-layer analysis in Figure 4e presents analyses of resistivities, thicknesses, and depths along the profile. DPH3 is the depth to the third layer, and DPH4 is the depth to the fourth layer. The depth to the second layer is equal to the thickness of the first layer. We see that the resistivity of the top two layers is well determined for most of the profile. The resistivity of the third and fourth layers is well determined when they are close to the surface (coordinate, 100–400 m). The thickness of the first layer is well determined for parts of the profile (e.g., coordinate, 250–400 m), whereas the thicknesses of the second and third layer are poorly resolved for most of the profile. Although the thicknesses of layers two and three are poorly determined for  $x_k < 500$  m, given an undoubtably strong anticorrelation we see that the depth to the fourth layer is fairly well determined for that part of the profile.

The strength of the lateral constraints, matrices  $C_{Rh}$  and  $C_p$  in equation (24), helps resolve the layer boundaries by constraining the depths and resistivities along the profile. Loose constraints allow model complexity only bounded by the data. Tight constraints make for a very smooth model with slow variations. Thus, determining the constraint values is a trade-off between fitting the data (complex models, no constraints) and fitting the lateral constraints (smooth models, tight constraints). One might argue that we are cheating because in this case we know the actual geological variations and thus choose the constraints accordingly. However, numerous exper-

iments on far more complex synthetic models (not shown here) show these settings to be appropriate for a large fraction of the models.

Finally, the starting model is in all cases a layered half-space (in this case, a four-layer model with the same resistivity in all of the layers), making the inversion scheme robust. Four layers were used in the LCI section as an inversion because three layers had a poorer data fit and five layers did not result in a significantly better data fit (models not shown here).

Based on this synthetic model, we conclude that the layered solution has clear advantages over the smooth minimum-structure solution when the geological model is quasi-layered. The result can be evaluated using the sensitivity analysis and the straightforward identification of layered units.

### FIELD EXAMPLE, CVES, SWEDEN

Figure 5 is a CVES field example from Sweden. The profile is approximately 300 m. The resistivity survey was carried out as part of a geotechnical investigation for road construction in connection with a filled basin structure in bedrock. The data set is presented by Dahlin (1996). The data pseudosection in Figure 5a shows relatively smooth transitions but with clear indications of 2D structures. The data are collected using Wenner arrays, with  $a$ -spacing between 2 and 48 m.

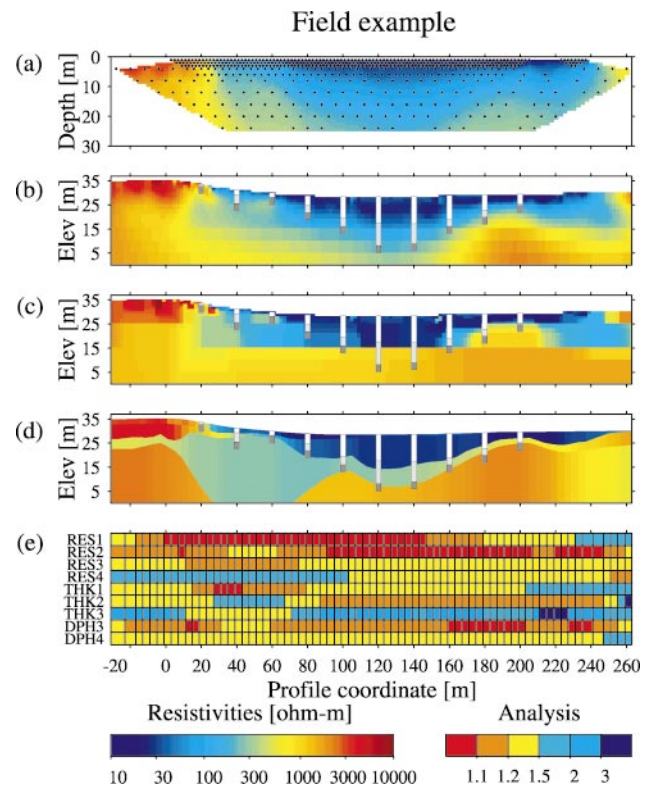


Figure 5. (a) The data pseudosection. (b) The minimum structure L2 norm inversion result. (c) The corresponding L1 norm inversion result. (d) The 2D LCI result with the parameter analyses in (e). The color-coding of the analyses ranges from well resolved (red) to poorly resolved (blue). Lithological logs from drillings are located every 20 m from coordinate 20 to 200 m. The colors of the drillholes indicate, from the bottom, rock (dark gray), till (light gray), and clay (white).

The L2 norm model in Figure 5b picks up a basin structure, thickest around coordinate 120–130 m. The identification of all three layers depicted in the drillholes is impossible, and the depth to bedrock is not easily identified, although the overall model geometry reflects the drill data to some degree. For the left half of the profile, it seems that the rock identified in the drillholes is of a different character from the rock detected on the right half of the profile based on prominent differences in resistivity. This is most likely from 3D structures (Dahlin, 1996). The L1 norm model of Figure 5c is more blocky than the L2 norm model, but still the formations depicted by the drillholes are not picked up.

Figure 5d presents a 2D LCI section with four layers. No a priori information is added. The basin unit is now clearly separated from the bedrock, and for the right half of the profile (coordinates 100–230 m) the till unit is easily identified on top of the bedrock. The thicknesses of the clay layer and the till–clay layer are fairly consistent with those found in the drillholes. For the left half of the profile there are inconsistencies, as was the case for the L2 norm model of Figure 5b. We pick up the till layer at coordinate 40 m, but it is not possible to track the layer between coordinates 40 and 100 m.

The analyses in Figure 5d show mainly well-determined resistivities for the entire profile for layers 1 and 2, whereas the bottom two layers have only moderately resolved resistivities. The thicknesses of the till layer (THK3, coordinates 100–230 m) is poorly resolved, but the depth to the top of the till (DPH3), i.e., the basin depth, is well determined. The model sections produce data that fit the observed data to an acceptable level according to the relevant inversion scheme.

#### CVES FIELD EXAMPLE WITH A PRIORI INFORMATION, SWEDEN

Figure 6 is a CVES field example from a geotechnical slope stability investigation in Sweden (Wisen et al., 2003). The full profile is approximately 200 m. The geological environment consists of crystalline bedrock overlain by a layer of sand and silt till with a thickness from zero up to a few meters. On top of the sand–silt till are several meters of unconsolidated clay. The depth to the surface of the bedrock was established from a refraction seismic survey.

In Figure 6a the data are presented, showing relatively smooth transitions. A combination of Wenner and Schlumberger electrode configurations was used with a minimum electrode distance of 2 m.

The L2 norm model in Figure 6b picks up the overall downward-ascending resistivity structures but fails to identify a separate sand unit. The depth to the bedrock as indicated by the refraction seismic data is much deeper than the high-resistivity contrast of the smooth L2 norm inversion. This suggests that the sand–silt till is a hidden layer on top of the bedrock. The L1 norm model (Figure 6c) is much more blocky than the L2 norm model, but still the sand–silt till is not detected.

Figure 6d is the 2D LCI section with four layers and no a priori information. A thin unit is seen on top of the bedrock that could correspond to the sand–silt till, but it is quite far from the boundary, as suggested by the refraction seismic. In Figure 6e the depth to the bedrock has been added as a priori information in the 2D LCI algorithm. This reveals a relatively thick unit on top of the bedrock with a slightly lower resistivity than that of

the bedrock. Figures 6d and 6e fit the data to the same degree, which means that the refraction seismic and resistivity data do not in any way contain contradicting information, as one might think by looking at Figures 6b–6d. Also, by including the a priori information on the depth to the bedrock, we are able to retrieve supplementary information on the thickness and resistivity of the sand–silt layer.

#### DISCUSSION

##### Smooth minimum structure or discrete layers?

As seen from the examples, a smooth minimum-structure L2 norm inversion produces smooth models even for geological models, which are overall layered. For an L1 norm solution the models are more blocky but still fail to identify quasi-layered units. The question is when to use a smooth minimum-structure solution and when to use a solution with discrete

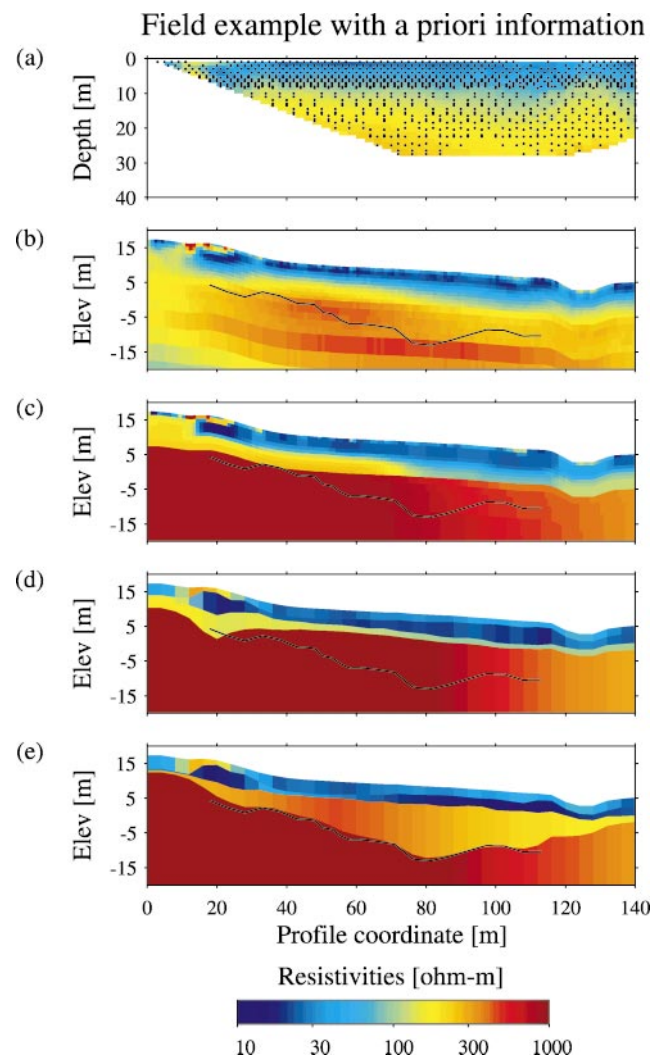


Figure 6. (a) The data pseudosection. (b) The minimum-structure L2 norm inversion result. (c) The corresponding L1 norm inversion result. (d) The 2D LCI result without a priori information. (e) Includes depth to the bedrock as a priori information. The depth to the bedrock from the refraction seismic data is drawn as a black line.

layers. Often an interpreter has some background knowledge on the area in terms of distinct units with different electrical properties. We suggest the use of the 2D LCI whenever these units take the form of a quasi-layered environment. When they are not quasi-layered, a minimum-structure solution should be used.

### Code optimizing

The 2D forward solution is significantly slower to use than the 1D forward solution. For long profiles this difference becomes even more pronounced. Therefore, it is preferable to use the 2D code only when the subsurface geometry is not approximately one dimensional. The 2D LCI as presented here is implemented in an inversion kernel developed for 1D LCI by adding the 2D resistivity forward routine to the other forward routines in the program. This feature enables us to examine hybrid forms in which parts of the calculations are one dimensional and others are two dimensional. One possible hybrid is to do 1D calculations for the first few iterations and then shift to 2D calculations when the basic structures have been built (Christiansen and Auken, 2003).

Other considerations to make a faster code include the dual grid method of Torres-Verdin et al. (2000) or a form of Broyden's update (quasi-Newton) for Jacobian calculation (Loke and Barker, 1996). Also, one could use a fast approximate 2D inversion to get a suitable starting model for the full nonlinear inversion (Møller et al., 2001).

### CONCLUSION

The 2D LCI inversion of continuous resistivity data has proven to be a robust tool to obtain reliable inversion results in quasi-layered environments. The layered model parameterization allows easy identification of formation boundaries, compared to a standard minimum-structure 2D program which produces a more smeared picture of the geological model. The inclusion of lateral constraints improves the resolution of poorly resolved parameters. We have demonstrated this on a synthetic data set, comparing inverted sections from the 2D LCI method with 2D minimum-structure models. In a field example from Sweden, a till layer hidden in the smooth minimum-structure section was identified using the 2D LCI method and confirmed by drillholes.

A priori knowledge can be added at any point along the model profile, and the results are supported by a full sensitivity analysis of the model parameters entering the inversion scheme. Thus, the interpreter is given a chance to evaluate the inversion result.

### ACKNOWLEDGMENTS

We thank Douglas Oldenburg, University of British Columbia, Canada, for use of his 2D resistivity code in our implementation. The field data were kindly provided by Torleif Dahlin, University of Lund, Sweden. Torquil Smith, Lawrence Berkeley National Laboratory, Berkeley, California, helped us start the project at the very beginning. Bo Holm Jacobsen and Niels B. Christensen, University of Aarhus, Denmark, helped clarify the paper and contributed numerous helpful comments. Colin Farquharson, two anonymous reviewers, and associate

editor Louise Pellerin gave insightful comments that improved the paper significantly. Lone Davidsen assisted in the English language editing.

## APPENDIX A

### DERIVATIVES ON A PRIORI DEPTHS AND DEPTH CONSTRAINTS

In equation (15) we added a priori information on depths to the inverse formulation. With the a priori depths added to the system, we must also add the derivatives of the depths from the primary model parameters to build the matrix  $\mathbf{P}_h$ . The derivatives with respect to resistivities are all zero. The derivatives with respect to layer thicknesses at horizontal position  $x_k$  are

$$\begin{aligned} \frac{\partial \log(h_{k,l})}{\partial \log(t_{i,j})} &= \frac{t_{i,j}}{h_{k,l}} \cdot \frac{\partial h_{k,l}}{\partial t_{i,j}} = \frac{t_{i,j}}{h_{k,l}} \cdot \frac{\partial \sum_{s=1}^l t_{k,s}}{\partial t_{i,j}} \\ &= \begin{cases} \frac{t_{i,j}}{h_{i,j}} & \text{for } i=k \text{ and } j \leq l \\ 0 & \text{otherwise} \end{cases} \quad (\text{A-1}) \end{aligned}$$

for the  $l$ th depth with respect to the  $j$ th thickness. Now, we write out the elements of the  $\mathbf{P}_h$  matrix with respect to the submodel at  $x_k$ :

$$\mathbf{P}_h = \begin{bmatrix} \dots & 0 & \dots & 0 & 1 & 0 & 0 & \dots & 0 & \dots \\ \dots & 0 & \dots & 0 & \frac{t_{k,1}}{h_{k,2}} & \frac{t_{k,2}}{h_{k,2}} & 0 & \dots & 0 & \dots \\ & & \vdots & \vdots & \vdots & \vdots & & & & \vdots \\ \dots & 0 & \dots & 0 & \frac{t_{k,1}}{h_{k,n}} & \frac{t_{k,2}}{h_{k,n}} & \frac{t_{k,3}}{h_{k,n}} & \dots & \frac{t_{k,n}}{h_{k,n}} & \dots \end{bmatrix} \quad (\text{A-2})$$

for the  $n$  a priori depths using the identity  $t_{1,1} = h_{1,1}$ . The first  $n_l$  columns of zeroes are the derivatives with respect to resistivities. The variance on the a priori depths will enter as  $\mathbf{C}_{h-prior}$ , which we take to be a diagonal matrix.

Next, we need to find the derivatives with respect to depths to build the matrix  $\mathbf{R}_h$ . Similar to equation (A-1), the constraints on submodels at  $x_k$  and  $x_{k+1}$  have derivatives with respect to thicknesses given as

$$\begin{aligned} \frac{\partial (\log(h_{k,l}) - \log(h_{k+1,l}))}{\partial \log(t_{i,j})} &= \frac{\partial \log(h_{k,l})}{\partial \log(t_{i,j})} - \frac{\partial \log(h_{k+1,l})}{\partial \log(t_{i,j})} \\ &= \frac{t_{i,j}}{h_{k,l}} \cdot \frac{\partial \sum_{s=1}^l t_{k,s}}{\partial t_{i,j}} - \frac{t_{i,j}}{h_{k+1,l}} \cdot \frac{\partial \sum_{s=1}^l t_{k+1,s}}{\partial t_{i,j}} \\ &= \begin{cases} \frac{t_{i,j}}{h_{i,j}} - \frac{t_{i+1,j}}{h_{i+1,j}} & \text{for } i=k \text{ and } j \leq l \\ 0 & \text{otherwise} \end{cases} \quad (\text{A-3}) \end{aligned}$$

for the  $l$ th depth with respect to the  $j$ th thickness in submodels  $k$  and  $k+1$ . The full matrix with derivatives of depth constraints

then becomes

$$R_h = \begin{bmatrix} \dots & 0 & \dots & 0 & 1 & 0 & 0 & \dots & 0 & \dots \\ \dots & 0 & \dots & 0 & \frac{t_{k,1}}{h_{k,2}} & \frac{t_{k,2}}{h_{k,2}} & 0 & \dots & 0 & \dots \\ & \vdots & & \vdots & \vdots & \vdots & & & \vdots & \\ \dots & 0 & \dots & 0 & \frac{t_{k,1}}{h_{k,n}} & \frac{t_{k,2}}{h_{k,n}} & \frac{t_{k,3}}{h_{k,n}} & \dots & \frac{t_{k,n}}{h_{k,n}} & \dots \\ & \dots & 0 & \dots & 0 & -1 & 0 & 0 & \dots & 0 & \dots \\ & \dots & 0 & \dots & 0 & -\frac{t_{k+1,1}}{h_{k+1,2}} & -\frac{t_{k+1,2}}{h_{k+1,2}} & 0 & \dots & 0 & \dots \\ & & \vdots & & \vdots & \vdots & \vdots & & \vdots & & \\ & \dots & 0 & \dots & 0 & -\frac{t_{k+1,1}}{h_{k+1,n}} & -\frac{t_{k+1,2}}{h_{k+1,n}} & -\frac{t_{k+1,3}}{h_{k+1,n}} & \dots & -\frac{t_{k+1,n}}{h_{k+1,n}} & \dots \end{bmatrix}. \quad (\text{A-4})$$

Again, the first columns with zeroes are derivatives with respect to resistivities. The variances on the lateral constraints are given in  $\mathbf{C}_{Rh}$ .

## APPENDIX B

### THE FULL ITERATIVE INVERSION SCHEME

In equation (25) we wrote the solution to the inverse problem as

$$\delta \mathbf{m}_{est} = [\mathbf{G}'^T \mathbf{C}'^{-1} \mathbf{G}']^{-1} \mathbf{G}'^T \mathbf{C}'^{-1} \delta \mathbf{d}', \quad (\text{B-1})$$

with respect to some reference model  $\mathbf{m}_{ref}$ . Writing this as the model update at the  $n$ th iteration in an iterative inversion scheme, we get

$$\mathbf{m}_{n+1} = \mathbf{m}_n + ([\mathbf{G}_n'^T \mathbf{C}'^{-1} \mathbf{G}_n' + \lambda_n \mathbf{I}]^{-1} \cdot [\mathbf{G}_n'^T \mathbf{C}'^{-1} \delta \mathbf{d}'_n]), \quad (\text{B-2})$$

where  $\lambda$ , is a Marquart damping parameter (Marquart, 1963). Expanding equation (B-2) with respect to equations (22) and (24), we end up with

$$\begin{aligned} \mathbf{m}_{n+1} = \mathbf{m}_n &+ ([\mathbf{G}^T \mathbf{C}_{obs}^{-1} \mathbf{G} + \mathbf{C}_{prior}^{-1} + \mathbf{P}_h^T \mathbf{C}_{h-prior}^{-1} \mathbf{P}_h \\ &+ \mathbf{R}_p^T \mathbf{C}_{Rp}^{-1} \mathbf{R}_p + \mathbf{R}_h^T \mathbf{C}_{Rh}^{-1} \mathbf{R}_h + \lambda_n \mathbf{I}]^{-1} \\ &\cdot [\mathbf{G}^T \mathbf{C}_{obs}^{-1} (\mathbf{d}_{obs} - \mathbf{g}(\mathbf{m}_n)) + \mathbf{C}_{prior}^{-1} (\mathbf{m}_{prior} - \mathbf{m}_n) \\ &+ \mathbf{P}_h \mathbf{C}_{h-prior}^{-1} (\mathbf{h}_{prior} - \mathbf{P}_h \mathbf{m}_n) + \mathbf{R}_p^T \mathbf{C}_{Rp}^{-1} (-\mathbf{R}_p \mathbf{m}_n) \\ &+ \mathbf{R}_h^T \mathbf{C}_{Rh}^{-1} (-\mathbf{R}_h \mathbf{m}_n)]), \quad (\text{B-3}) \end{aligned}$$

where  $\mathbf{g}(\mathbf{m}_n)$  is the nonlinear forward response of the  $n$ th model. The convergence of the inversion process is stabilized by two processes: (1) the Marquart modification via the parameter  $\lambda_n$  and (2) an adaptive damping on the step size for the model update based on the success of the previous iteration. These two factors make the inversion process very robust. In practice, we achieve safe convergence by starting the iteration

from horizontal layers with equal resistivities, i.e., a layered homogeneous half-space.

## REFERENCES

- Auken, E., Foged, N., and Sørensen, K. I., 2002, Model recognition by 1-D laterally constrained inversion of resistivity data: 9th Meeting, Environmental and Engineering Geophysical Society—European Section, Proceedings, 241–244.
- Bernstone, C., and Dahlin, T., 1999, Assessment of two automated DC resistivity data acquisition systems for landfill location surveys: Two case studies: Journal of Environmental and Engineering Geophysics, **4**, No. 2, 113–121.
- Christensen, N. B., and Sørensen, K. I., 1998, Surface and borehole electric and electromagnetic methods for hydrogeological investigations: European Journal of Environmental and Engineering Geophysics, **3**, 75–90.
- Christiansen, A. V., and Auken, E., 2003, Optimizing the 2D laterally constrained inversion (2D-LCI) using a quasi-Newton method and 1D derivatives: 9th Meeting, Environmental and Engineering Geophysical Society, European Section, Proceedings, O-030.
- Dahlin, T., 1996, 2D resistivity surveying for environmental and engineering applications: First Break, **14**, No. 7, 275–283.
- Dey, A., and Morrison, H. F., 1979, Resistivity modeling for arbitrarily shaped two-dimensional structures: Geophysical Prospecting, **27**, 106–136.
- Farquharson, C. G., and Oldenburg, D. W., 1998, Non-linear inversion using general measures of data misfit and model structure: Geophysical Journal International, **134**, 213–227.
- , 2003, Constructing piece-wise-constant models using general measures in non-linear, minimum-structure inversion algorithms: 6th International Symposium, Society of Exploration Geophysicists of Japan, Proceedings.
- Jackson, D. D., 1979, The use of a priori data to resolve non-uniqueness in linear inversion: Geophysical Journal of the Royal Astronomical Society, **57**, 137–157.
- Johansen, H. K., 1977, A man/computer interpretation system for resistivity soundings over a horizontally stratified earth: Geophysical Prospecting, **25**, 667–691.
- Loke, M. H., and Barker, R. D., 1996, Rapid least-squares inversion of apparent resistivity pseudosections by a quasi-Newton method: Geophysical Prospecting, **44**, 131–152.
- Loke, M. H., Acworth, I., and Dahlin, T., 2001, A comparison of smooth and blocky inversion methods in 2-D electrical imaging surveys: 15th Geophysical Conference, Australian Society of Exploration Geophysicists, Preview, **93**, 90–91.
- Marquart, D., 1963, An algorithm for least squares estimation of nonlinear parameters: SIAM, Journal of Applied Mathematics, **11**, 431–441.
- McGillivray, P., 1992, Forward modeling and inversion of dc resistivity and mmr data: Ph.D. thesis, University of British Columbia.
- Menke, W., 1989, Geophysical data analysis: Discrete inverse theory: Academic Press Inc.

- Møller, I., Jacobsen, B., and Christensen, N., 2001, Rapid inversion of 2-D geoelectrical data by multichannel deconvolution: *Geophysics*, **66**, 800–808.
- Olayinka, A. I., and Yaramanci, U., 2000, Use of block inversion in the 2-D interpretation of apparent resistivity data and its comparison with smooth inversion: *Journal of Applied Geophysics*, **45**, 63–81.
- Oldenburg, D. W., and Li, Y., 1994, Inversion of induced polarization data: *Geophysics*, **59**, 1327–1341.
- Panissod, C., Lajarthe, M., and Tabbagh, A., 1997, Potential focusing: A new multielectrode array concept, simulating study, and field tests in archaeological prospecting: *Journal of Applied Geophysics*, **38**, 1–23.
- Smith, J. T., Hoversten, M., Gasperikova, E., and Morrison, F., 1999, Sharp boundary inversion of 2D magnetotelluric data: *Geophysical Prospecting*, **47**, 469–486.
- Sørensen, K. I., 1996, Pulled array continuous electrical profiling: *First Break*, **14**, 85–90.
- Tarantola, A., and Valette, B., 1982, Generalized non-linear inverse problems solved using the least squares criterion: *Reviews of Geophysics and Space Physics*, **20**, No. 2, 219–232.
- Torres-Verdin, C., Druskin, V. L., Fang, S., Knizhnerman, L. A., and Malinverno, A., 2000, A dual-grid nonlinear inversion technique with applications to the interpretation of dc resistivity data: *Geophysics*, **65**, 1733–1745.
- Van Overmeeren, R. A., and Ritsema, I. L., 1988, Continuous vertical electrical sounding: *First Break*, **6**, 313–324.
- Ward, S. H., and Hohmann, G. W., 1987, Electromagnetic theory for geophysical applications *in* Nabighian, M. N., Ed., *Electromagnetic methods in applied geophysics*: Society of Exploration Geophysics, 131–312.
- Wisén, R., Christiansen, A. V., Auken, E., and Dahlin, T., 2003, Application of 2D laterally constrained inversion and 2D smooth inversion of CVES resistivity data in a slope stability investigation: 9th Meeting, Environmental and Engineering Geophysical Society, European Section, Proceedings O-002.